ResearchGate

See discussions, stats, and author profiles for this publication at: https://www.researchgate.net/publication/265550000

Contrasting Effects of Nanoparticle Binding on Protein Denaturation

ARTICLE *in* THE JOURNAL OF PHYSICAL CHEMISTRY C · AUGUST 2014

Impact Factor: 4.77 · DOI: 10.1021/jp506135m

CITATIONS
3

READS
35

8 AUTHORS, INCLUDING:

Katsuo Kurabayashi
University of Michigan
137 PUBLICATIONS **1,682** CITATIONS
SEE PROFILE

Amanda S Barnard
The Commonwealth Scientific and Industrial …
181 PUBLICATIONS **4,318** CITATIONS
SEE PROFILE

David Alan Winkler
The Commonwealth Scientific and Industrial …
166 PUBLICATIONS **2,527** CITATIONS
SEE PROFILE

Pu Chun Ke
Monash University (Australia)
99 PUBLICATIONS **2,297** CITATIONS
SEE PROFILE

Available from: Amanda S Barnard
Retrieved on: 31 January 2016

THE JOURNAL OF PHYSICAL CHEMISTRY C

Article

pubs.acs.org/JPCC

Contrasting Effects of Nanoparticle Binding on Protein Denaturation

Pengyu Chen,[†] Shane A. Seabrook,[‡] V. Chandana Epa,[‡] Katsuo Kurabayashi,[†] Amanda S. Barnard,[‡] David A. Winkler,*[,§,∥] Jason K. Kirby,*[,¶] and Pu Chun Ke*[,‡]

[†]Department of Mechanical Engineering, University of Michigan, Ann Arbor, Michigan 48109, United States

[‡]CSIRO Materials Science and Engineering, 343 Royal Parade, Parkville, VIC 3052, Australia

[§]CSIRO Materials Science and Engineering, Bayview Avenue, Clayton, VIC 3168, Australia

[∥]Monash Institute of Pharmaceutical Sciences, 390 Royal Parade, Parkville, VIC 3052, Australia

[¶]CSIRO Land and Water, Waite Road-Gate 4, Glen Osmond, SA 5064, Australia

Supporting Information

ABSTRACT: Understanding the interactions between nanoparticles (NPs) and proteins is essential for the design of bionanotechnology and biomedicine and for delineating the biological implications of nanomaterials for safe nanotechnology. In the present study we have examined protein denaturation in the presence of NPs, using the high-throughput technique of differential scanning fluorometry. Specifically, the melting temperature of human immunoglobulin (IgG) rose from 59.5 to 68.5 °C while that of lysozyme dropped from 74.0 to 68.8 °C for increasing NP:protein molar ratios. This contrast in protein stability was further examined by circular dichroism spectroscopy and Thioflavin T measurements, where a marked increase in β-sheets as well as amyloid fibrillation occurred in lysozyme while small changes were seen in the secondary structure of IgG. Our immunoassays further revealed a greatly elevated cytokine production in the cells treated with fullerol-lysozyme and a mostly unchanged TNF-α secretion in THP-1 cells exposed to fullerol-IgG, suggesting a connection between changes in protein secondary structure induced by fullerol binding and their triggered immune responses. These contrasting effects imply that, due to their finite solubility and size NPs display the duality of both a particle and a chemical and, therefore, do not conform to the conventional role of a ligand in protein stabilization.

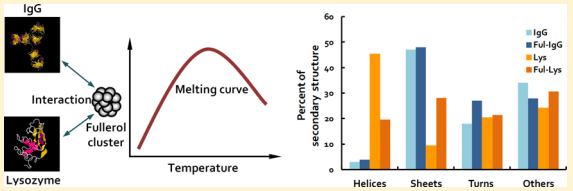

INTRODUCTION

Since its inception in the 1980s, nanotechnology has been increasingly integrated into many facets of modern science, technology, and manufacturing. It is now understood that the unique physical and physicochemical properties of nanomaterials, such as their large surface area to volume ratio and high reactivity, can give rise to a host of complex phenomena on the nanoscale that disobey scaling laws.[1] When introduced into biological systems, nanomaterials have shown a great potential for the application in medicine and biotechnology, yet such potential is often compromised by concerns over nanotoxicity and the lack of knowledge on how nanomaterials and living systems interact.[2] Fundamental to understanding the biological implications of nanotechnology is the elucidation of the interfacial phenomena between nanoparticles (NPs) and biomolecules. Such molecular insight complements the "big data" obtained from top-down approaches at the cellular and organism levels.[3]

The most common and important form of NP−biomolecular interactions usually involves proteins of the cell and blood plasma, whose prevalence, versatile functionality, and amphiphilicity conjures up a protein "corona" that underlies the biological identity of the NP.[4] It is now understood that proteins can readily coat the NP surface through physical adsorption and electrostatic and hydrophobic interactions. The resulting NP-protein entity may be retained for a short (i.e., "soft" corona) or extended (i.e., "hard" corona) time driven by thermodynamics and the Vroman effect dictated by protein binding affinity for the NP.[4,5] Despite the increasing knowledge that is available on the cytotoxicity elicited by the NP-protein corona, it is poorly understood how the physical association of NPs and proteins may impact the stability, aggregation, and function of the proteins that entail further biological and biomedicinal consequences.[4,6−10]

The current experimental strategies for examining NP−protein interactions employ a range of analytical and biophysical techniques, including gel electrophoresis, UV−vis spectrophotometry, Fourier transform infrared spectroscopy, Raman spectroscopy, circular dichroism (CD) spectroscopy, mass spectroscopy, surface plasmon resonance, hyperspectral imaging, electron microscopy, dynamic light scattering (DLS), and isothermal titration calorimetry, among others.[4,6−9] Most of these techniques, however, are low throughput, require intensive and expensive sample preparations, and are often operated under invasive or dehydrated conditions inconsistent with the actual NP-protein binding event. In this study we

Received: June 20, 2014
Revised: August 21, 2014
Published: August 26, 2014

© 2014 American Chemical Society

dx.doi.org/10.1021/jp506135m | J. Phys. Chem. C 2014, 118, 22069−22078

Scheme 1[a]

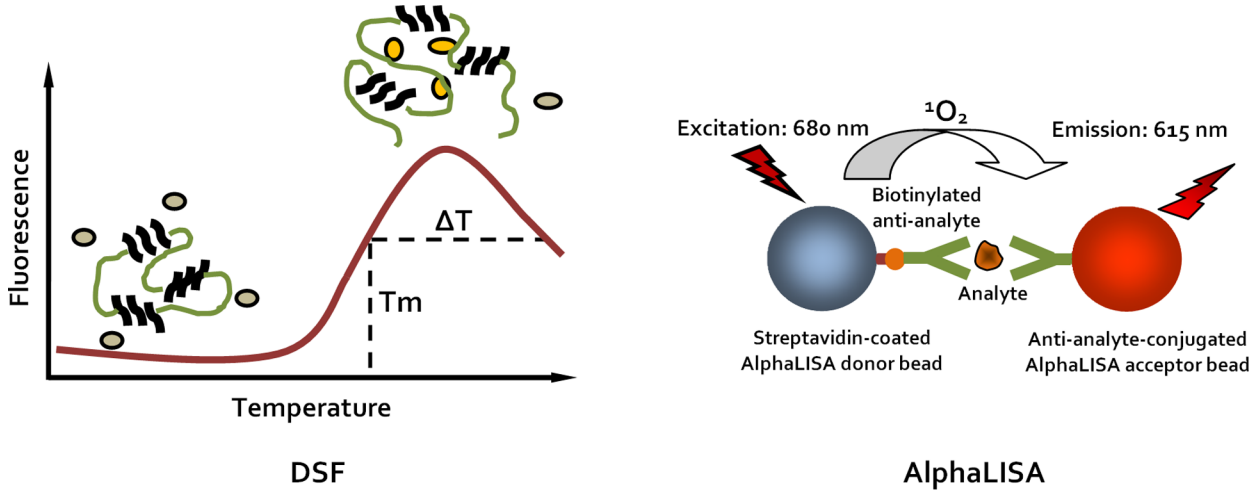

[a]Left: Protein melting curve vs temperature measured by DSF, from the folded state where the hydrophobic fluorophores are excluded to the molten state where fluorophores are integrated into the protein hydrophobic core to emit a strong fluorescence. The melting temperature T_m corresponds to the temperature where the increase in fluorescence is the most rapid. Also illustrated is the range of transition temperature ΔT, a parameter describing protein denaturation from the molten state to the aggregated state. Right: Working principle of the AlphaLISA immunoassay, where cytokine TNF-α serves as the analyte.

examine the stability of proteins at elevated temperatures and in the presence of a fullerene derivative $C_{60}(OH)_{20}$, or fullerol, using a fluorescence-based thermal shift assay—differential scanning fluorometry (DSF),[11−13] that is operated on a desktop, high-throughput real-time polymerase chain reaction platform under hydrated conditions.

The working principle of DSF is centered on the employment of a hydrophobic fluorophore, such as Sypro Orange (Ex/Em: 300, 470 nm/570 nm). As a result of unfolding at increased temperatures the hydrophobic core of a molten protein of interest becomes exposed to the external environment.[11] Consequently the fluorophore binds to the protein core and, upon excitation, gives rise to fluorescence that is otherwise quenched by the aqueous solution. Further increases in temperature cause the proteins to form aggregates through intermolecular hydrophobic interactions, which in turn discourages incorporation of the fluorophore into the proteins to gradually cease fluorescence. The approximate midpoint between the fluorescence intensity minima and maxima on a sigmoidal melting curve where a largest slope occurs is defined as the apparent melting temperature T_m (refer to Scheme 1), which in DSF is used as a primary indicator of protein stability.[11−13]

The proteins used in this study are immunoglobulin (IgG) and lysozyme. IgG is the most abundant antibody isotype in the blood and extracellular fluid, and a major protein involved in the immune response of the cell by binding to a host of pathogens to prevent infection. Structurally IgG consists of 2 identical heavy peptide chains and 2 identical light chains organized into a Y shape of ∼150 kDa, with its top two fragments for antigen binding (Fabs) and its tail (Fc) for the binding of cell membrane receptors. Lysozyme, in comparison, is a much smaller enzyme of ∼14 kDa that is abundant in the secretions of human milk, mucus, and tears. It is responsible for the breakage of peptidoglycans in the bacterial cell wall. IgG and lysozyme are selected as the model proteins in this study because of their biological relevance, disparate size, and similarities in charge and hydrophobicity. The relatively good solubility, rich biophysical properties, and medicinal potential[14−16] justifies fullerol as the NP of choice in the current study.

In addition to DSF for the characterization of protein stability in the presence of NPs, the hydrodynamic sizes and surface charges of IgG, lysozyme, and fullerol were determined using DLS. The mechanisms and energies for IgG and lysozyme binding by fullerol were probed by molecular docking simulations. Changes in the secondary structures of IgG and lysozyme induced by fullerol were quantified by CD spectroscopy, and amyloid fibrillation in the proteins exposed to fullerol was examined using a Thioflavin T assay. Furthermore, to gain an understanding of the effects of NP-protein binding on cell receptors and their activated signaling pathways we exposed THP-1 human acute monocytic leukemia cells to fullerol-IgG and fullerol-lysozyme and quantified secretion of the proinflammatory cytokine tumor necrosis factor-alpha (TNF-α). This study offers a new insight into NP−protein interactions versus temperature, a rarely studied and little understood aspect of nanoparticle−biomolecular binding, and provides an alternative strategy for evaluating the biological implications of nanomaterials.

RESULTS AND DISCUSSION

Hydrodynamic Size and Zeta Potential. While the hydrodynamic diameter of a fullerol molecule is known to be ∼1 nm,[3] the hydrodynamic diameter of a fullerol cluster determined by DLS was 66.4 ± 23.8 nm (upper tail ending at 150 nm; polydispersity index or PDI: 0.387) at room temperature due to fullerol self-assembly and aggregation, consistent with that reported in the literature.[17] The hydrodynamic diameters of the IgG and lysozyme were 10.3 ± 2.6 nm (PDI: 0.091) and 3.1 ± 0.7 nm (PDI: 0.029), respectively. In addition, the zeta potentials were determined at +7.00 ± 0.88 mV for IgG, +12.60 ± 2.60 mV for lysozyme, and −23.10 ± 2.23 mV for fullerol. In comparison, the zeta potentials for fullerol−IgG (100:1 molar ratio) and fullerol−lysozyme (10:1 molar ratio) were +1.86 ± 0.35 mV and +11.70 ± 1.24 mV,

dx.doi.org/10.1021/jp506135m | J. Phys. Chem. C 2014, 118, 22069−22078

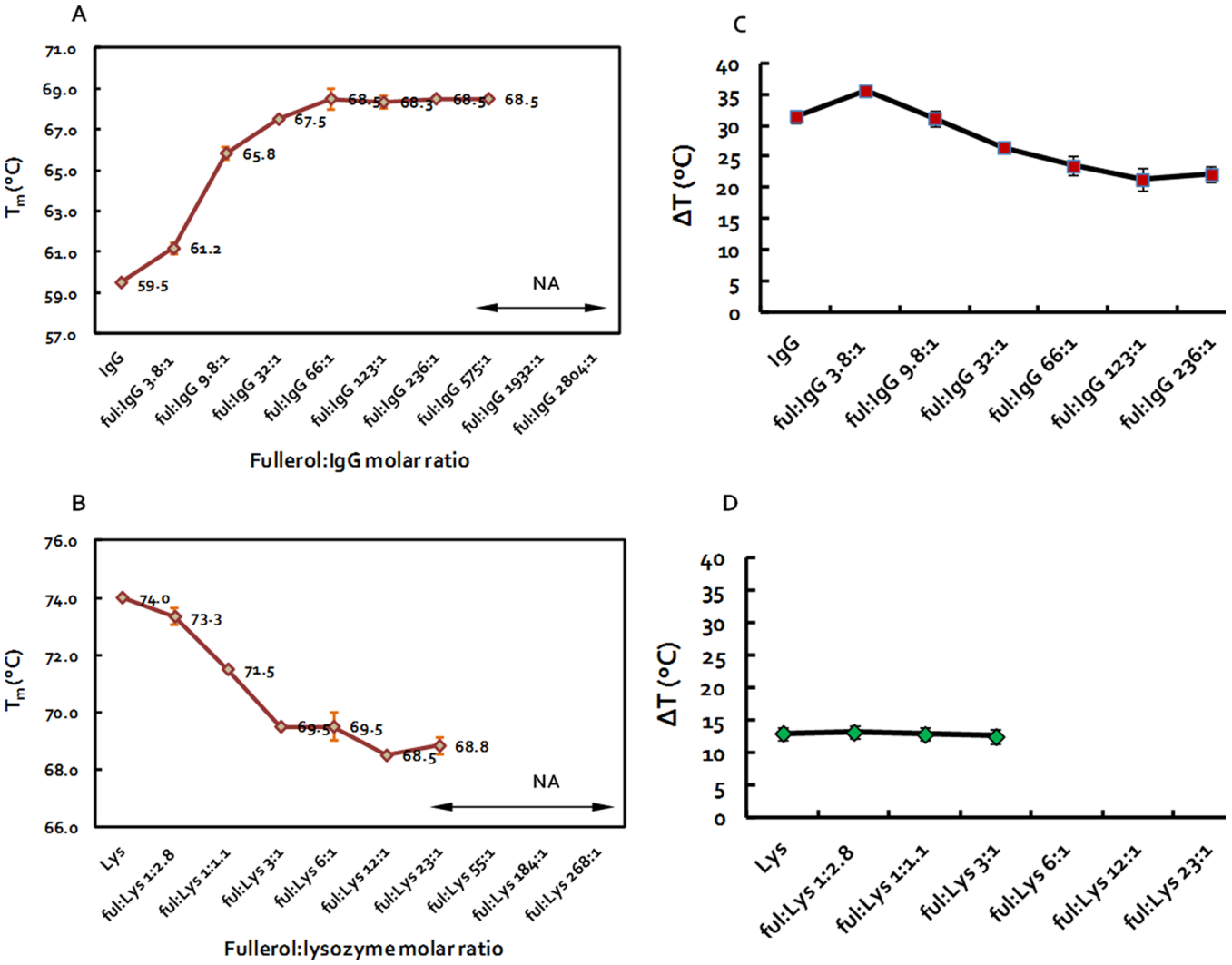

Figure 1. Melting temperatures of IgG (A) and lysozyme (B) in the presence of fullerol clusters of increasing NP:protein molar ratios. The corresponding ranges of transition temperature ΔT are shown in (C) and (D). NA: the range where T_m became unavailable due to low protein concentrations. ΔT became unavailable for fullerol:lysozyme molar ratios at 6:1 or higher in (D) due to multiphasic thermal transitions approaching the upper threshold of 100 °C. The plots of A–D were derived from the data shown in Supporting Information Figures S1 and S3.

respectively. This nearly neutral zeta potential of fullerol–IgG ranged between the zeta potentials of IgG and fullerol, excluding the possibility of an IgG corona fully encasing the fullerol cluster while pointing to a less organized NP-protein arrangement. In contrast, the zeta potential of fullerol–lysozyme closely resembled that of lysozyme alone, indicating coating of a lysozyme corona on the fullerol cluster.

Contrasting Behaviors of IgG and Lysozyme Melting upon Fullerol Binding. For the DSF measurements the molar ratio of fullerol:IgG was adjusted from 0:1 (i.e., IgG control) to 2804:1 while that of fullerol:lysozyme was increased from 0:1 (i.e., lysozyme control) to 268:1 using the stock protein solutions and NP suspensions. The selection of these molar ratios for the DSF measurements takes into account fullerol aggregation into fullerol clusters and the difference in the size of IgG and lysozyme. Specifically, assuming the radii of a fullerol molecule, a fullerol cluster, and a protein as ρ, R, and r, the approximate number of fullerol molecules that can be packed into a fullerol cluster is estimated as $((4/3\pi R^3)/(8\rho^3))$, while the total number of proteins adsorbed onto the surface of a fullerol cluster is calculated as $((4\pi(R + r)^2)/(\pi r^2))$.[18] On the basis of the hydrodynamic sizes measured for the fullerol cluster, IgG, and lysozyme we deduce that a fully coated fullerol cluster by IgG (abbreviated as "fullerol cluster-IgG'' hereafter for clarity, where applicable) corresponds to a molar ratio of ~100 fullerol molecules to 1 IgG (denoted as "fullerol:IgG = 100:1"), while a fully coated fullerol cluster by lysozyme (abbreviated as "fullerol cluster-lysozyme" hereafter, where applicable) requires a molar ratio of 10 fullerol molecules per lysozyme (denoted as "fullerol:lysozyme = 10:1"). Therefore, a molar ratio of fullerol:IgG higher or lower than 100:1 reflects a redundancy of fullerols or IgG, while a molar ratio of fullerol:lysozyme higher or lower than 10:1 indicates free fullerols or lysozyme in the suspension. Accordingly, our DSF designs (Figure 1) have considered sample conditions that encompass both redundant supplies of NPs and proteins in the NP–protein mixtures.

As shown in Figure 1A and Supporting Information Figure S1, the melting temperature of IgG increased monotonically from 59.5 °C for the protein control to 68.5 °C when the molar ratio of fullerol molecules to IgG was at 66:1. At higher molar ratios up to 575:1 the melting temperatures of the IgG

dx.doi.org/10.1021/jp506135m | J. Phys. Chem. C 2014, 118, 22069–22078

remained stable at ~68.5 °C, indicating saturation of fullerol molecules free from their interactions with IgG. At further higher molar ratios no melting temperatures were derivable due to low protein concentrations and hence a diminished signal-to-noise ratio. This result indicates that IgG became more stable in the presence of fullerol, consistent with the general observation of enhanced protein stability in the presence of small ligands as a result of the coupling between protein unfolding and protein−ligand binding.[19,20] Since this type of IgG possesses a positive surface charge but a tripodal morphology that discourages extensive contact of the protein with a globular NP cluster, it is likely that the negatively charged fullerol, now in smaller clusters due to elevated temperatures (~40 nm in size at 70 °C, Supporting Information Figure S2), bound loosely to the protein periphery (and vice versa) through electrostatic interactions as well as hydrogen bonding mediated by the NP surface hydroxyls and the hydrogen-bond donors/acceptors of the protein. Such interactions should further reduce the size of the fullerol clusters while translating to an additional energy cost to free the protein from the NPs in proximity. This is reflected by the increased IgG melting temperature with the augmented NP:protein molar ratio (Figure 1A) and by the comparability of such temperature increase-induced thermal energies with the strength of relevant hydrogen bonding (i.e., ~8−20 kJ/mol).[21]

The melting temperature of lysozyme displayed an entirely different trend in the presence of fullerol, i.e., an increased NP:protein molar ratio caused a decrease in the melting temperature of lysozyme (Figure 1B and Supporting Information Figure S3). Specifically, the melting temperature for the lysozyme control was 74.0 °C, consistent with that reported in the literature.[22] As the NP:protein molar ratio was increased to 6:1 the melting temperature of lysozyme was decreased to ~69.5 °C. Further increases in the molar ratio resulted in the melting temperature of the enzyme asymptoting to ~68.5 °C (Figure 1B), likely due to the accumulation of free fullerol molecules. No more data points were available beyond the molar ratio of 23:1 due to low protein concentrations. This trend indicates that the presence of fullerol clusters compromised the structure of lysozyme, likely through electrostatic attraction and hydrogen bonding between the two oppositely charged species. Due to the large disparity (an order of magnitude) in the size of lysozyme and the fullerol clusters, such interactions could, in principle, resemble the binding of small, cationic ubiquitin with anionic, citrate-coated silver NPs of 20 nm[23] or the adsorption of lysozyme onto silica beads of 20 and 100 nm,[24] both of which were reported to compromise the structure and activity of the proteins. Specifically, in the case of lysozyme adsorption onto silica beads[24] it was found that the larger silica beads of 100 nm induced a greater loss in lysozyme α-helices. This further reinforces the major role of size (as well as curvature) in NP−protein interactions[4] and validates our hypotheses on the contrasting effects of fullerol binding on IgG and lysozyme denaturation. These hypotheses are further supported by the zeta potential measurement, which pointed to a less organized arrangement for fullerol cluster-IgG and coating of a lysozyme corona on the fullerol cluster. Although beyond the focus of the present study, multiphasic thermal transitions[20] were observed occasionally in the DSF measurement (Supporting Information Figure S3). These suggest a greater complexity in fullerol cluster−lysozyme interactions due to the competing thermodynamics of NP−NP, NP−protein, and protein−protein interactions, especially at high NP concentrations.

In addition to T_m, the thermal stability of a protein is also manifested by its range of transition temperature ΔT in DSF (refer to Scheme 1). This parameter identifies the points from protein melting to intermolecular aggregation, accompanied by ejection of the fluorophores from the hydrophobic protein core to induce fluorescence quenching. As shown in Figure 1C and D, IgG alone and fullerol cluster-IgG were associated with ΔT values of 36.0 to 19.5 °C, while lysozyme alone and fullerol cluster−lysozyme were characterized by significantly smaller ΔT values of 13.5 to 12.5 °C. This observation implies that, despite the lower T_m value for IgG than lysozyme (59.5 °C vs 74 °C), denaturation of IgG (and IgG associated with fullerol) required larger thermal energy than that of lysozyme (and lysozyme associated with fullerol), in order to compensate for the greater entropic loss in unraveling the larger IgG hydrophobic core to initiate intermolecular protein aggregation. The hydrophobicities of IgG and lysozyme are comparable, at 36.97% and 40.94%, respectively, as calculated using the Protein Data Bank (PDB) structures and the Peptide Property Calculator (freeware, LifeTein).

It is known that the structural stability of a protein depends upon the ionic strength of its solvent.[25] Therefore, the melting temperatures of IgG and lysozyme were measured against NaCl of different concentrations for a fixed fullerol:protein molar ratio of 3:1 (Figures 2, Supporting Information Figures S4 and S5). As shown in Figure 2A, the melting temperature of IgG (green curve) was reduced slightly from 60.0 °C for the control (i.e., without salt) to 59.0 °C for a 260 mM NaCl solution, followed by a significant reduction in T_m for a 453 mM NaCl solution. Similarly, the melting temperature of lysozyme decreased monotonically with increased NaCl concentration up to 385 mM (Figure 2B, green curve). These trends are consistent with the general observation that excess monovalent ions (over 150 mM for IgG and over 50 mM for lysozyme, according to the manufacturer) destabilize proteins as a result of screening and neutralization of the protein surface charge.[25] In addition, the melting temperature of IgG with fullerol was slightly reduced from 69.0 to 66.7 °C (Figure 2A, maroon curve), while the T_m of lysozyme with fullerol fluctuated between 69.5 and 70.2 °C with no statistical significance (Figure 2B, maroon curve). This result indicates the effect of fullerol in negating the impact of the salt ions on both types of proteins. In addition, multiphasic thermal transitions were observed (Supporting Information Figure S5) for fullerol cluster−lysozyme at high salt concentrations, reinforcing the competitive nature of NP−protein, NP−NP, and protein−protein interactions in reshaping the stability of small proteins.

Docking of Fullerol on IgG and Lysozyme. To further investigate the interaction mechanisms of fullerol and the proteins we computationally docked a fullerol molecule onto the appropriate sites of IgG and lysozyme. In the case of IgG this was to the antigen binding site at the CDR (complementarity determining regions) loops on one of the Fab regions, while in the case of lysozyme this was to the largest cavity on the protein molecular surface, i.e., the active-site cavity of the lysozyme. The results from these calculations are illustrated in Figure 3, showing for each protein the highest ranking (i.e., highest binding affinity between fullerol and the protein) docked pose of fullerol. In these docked poses fullerol makes specific hydrogen-bonding interactions with residues Asn 46, Thr 47, Asp 48, Asn 59, Trp 62, and Ala 107 of the

dx.doi.org/10.1021/jp506135m | J. Phys. Chem. C 2014, 118, 22069−22078

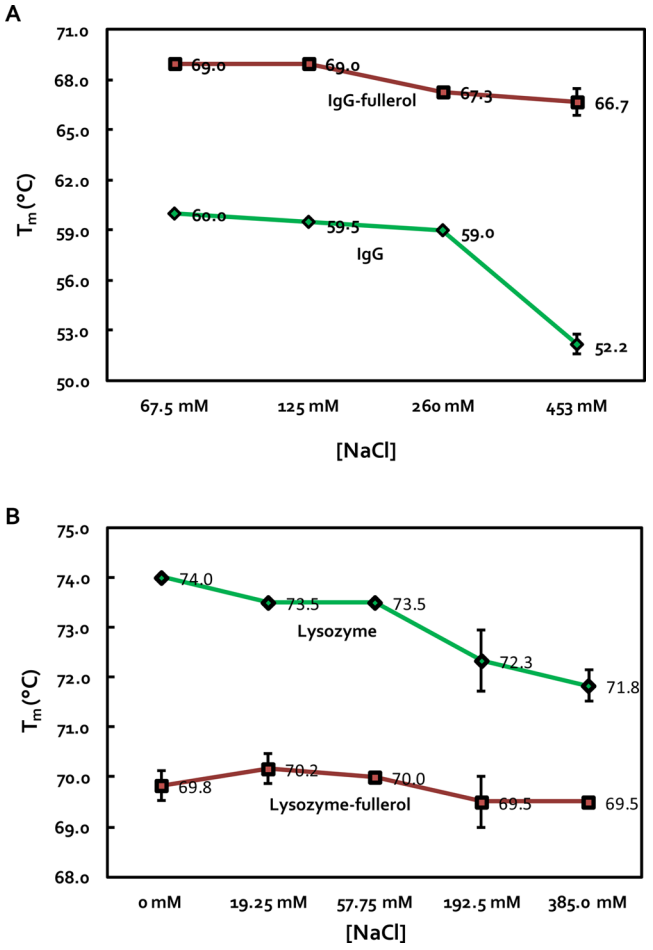

Figure 2. Melting temperatures of IgG (A) and lysozyme (B) (green curves) and their mixtures with fullerol clusters at a fixed NP:protein molar ratio of 3:1 (maroon curves). The plots were derived from the data shown in Supporting Information Figures S4 and S5.

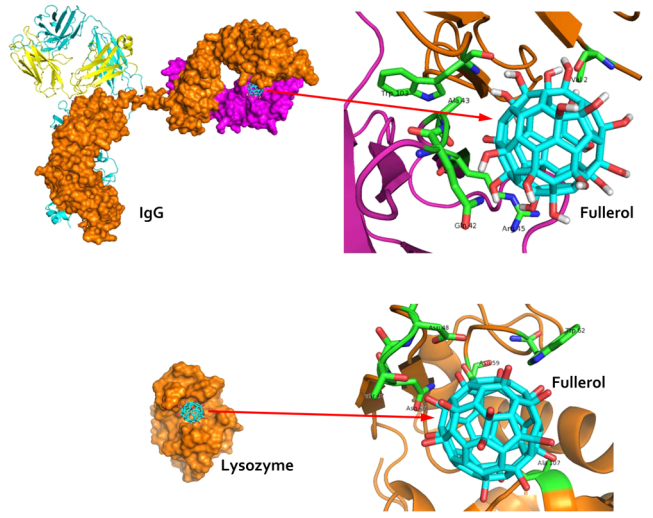

Figure 3. Illustrations of fullerol docking on IgG (top left) and lysozyme (bottom left). The enlarged right panels show the amino acid residues in the Fab domain of the IgG (top right; brown: heavy chain, purple: light chain) and the catalytic site of the lysozyme (bottom right) forming hydrogen bonds with the fullerol.

lysozyme, and with residues Val 2, Gln 42, Ala 43, Arg 45, and Trp 103 of the IgG, respectively. It is acknowledged that docking of a single fullerol molecule onto the proteins, here for the sake of a reduced computational cost, does not convey the rich phenomenon of protein sorption onto the surface of fullerol clusters. However, hydrogen bonding between the proteins and the fullerol molecule, as verified in the simulations, should still hold true as a component of the interaction mechanisms for the NP–protein systems under study.

Changes in Secondary Structures of IgG and Lysozyme Induced by Fullerol. CD spectroscopy is a powerful technique for assessing protein secondary structure, and hence was utilized for examining the structural information on IgG and lysozyme exposed to fullerol clusters. As shown in Figure 4, for IgG, a primarily β-sheeted protein, its CD spectra (light and dark blue traces in Figure 4A) remained nearly identical before and after incubation with fullerol. The predicted IgG secondary structure only displayed a variance in turns after binding with fullerol, indicating that the interaction between IgG and fullerol clusters did not induce notable structural changes but an increased hydrophobicity due to the presence of fullerol clusters, consistent with the DSF observation. In contrast, upon binding to fullerol clusters the α helix content of lysozyme displayed a marked 57% relative decrease (from 46% to 20%) while the β sheet content gained a 180% relative increase (from 10% to 28%) (Figure 4B). These contrasting conformational changes of IgG and lysozyme upon binding to fullerol clusters can be understood from the discrepancies in the physicochemical and structural characteristics of the two types of proteins as reflected by the DLS, zeta potential, DSF, and docking simulations. Specifically, the drastically increased β-sheet content in lysozyme is likely due to protein unfolding and aggregation promoted by fullerol cluster–lysozyme interaction, while protein aggregation is known to trigger inflammatory responses in a number of cases, such as Alzheimer's disease, Parkinson's disease, and type II diabetes.[26]

Amyloid Fibrillation in Lysozyme Exposed to Fullerol. Thioflavin T is a dye commonly used for the visualization and quantification of amyloid fibrillation induced by protein misfolding and aggregation.[27] When Thioflavin T binds to a cross-β sheet structure its fluorescence intensity is enhanced, which is often coupled with a redshift in its peak wavelength. Upon excitation of the Thioflavin T-stained samples at 440 nm, we noted a pronounced redshift of 16 nm coupled with an enhanced fluorescence signal of 15.9% for the sample of fullerol cluster–lysozyme at a molar ratio of 50:1 (Figure 5), compared with the fluorescence of Thioflavin T control. In comparison, a mere 2.9% of increase in fluorescence intensity coupled with no redshift was observed for fullerol cluster-IgG. This result indicates the formation of cross-β architecture and amyloid fibrils in lysozyme exposed to fullerol clusters, consistent with the CD experiment where a marked increase for α-helices and a significant decrease for β-sheets occurred for fullerol cluster–lysozyme.

Contrasting TNF-α Secretion in AlphaLISA Immunoassays. A number of recent studies have revealed that surface morphology and chemistry of NPs could result in physiological and pathological changes in protein conformation upon NP–protein interactions.[4,8,16,23,28,29] The unfolding of proteins impacts their interactions with surface receptors on immune cells that may activate the signaling pathway and trigger subsequent immune inflammatory response.[10,30] It is known

dx.doi.org/10.1021/jp506135m | J. Phys. Chem. C 2014, 118, 22069–22078

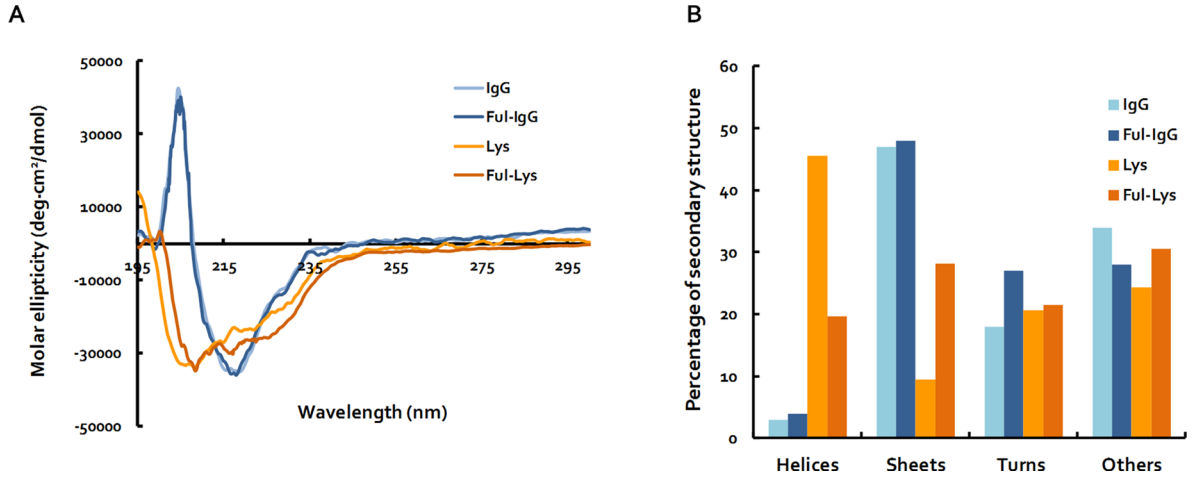

Figure 4. (A) CD spectra of IgG (0.1 mg/mL), lysozyme (0.01 mg/mL), and the proteins mixed with fullerol clusters (0.03 mg/mL) corresponding to a 50:1 NP:protein molar ratio. (B) Changes of IgG and lysozyme secondary structures upon binding with the fullerol clusters. The percentages of the secondary structures were calculated by the CDSSTR and CONTIN/LL algorithms of the CDPro package, using SMP56 and SP43 protein reference data sets.

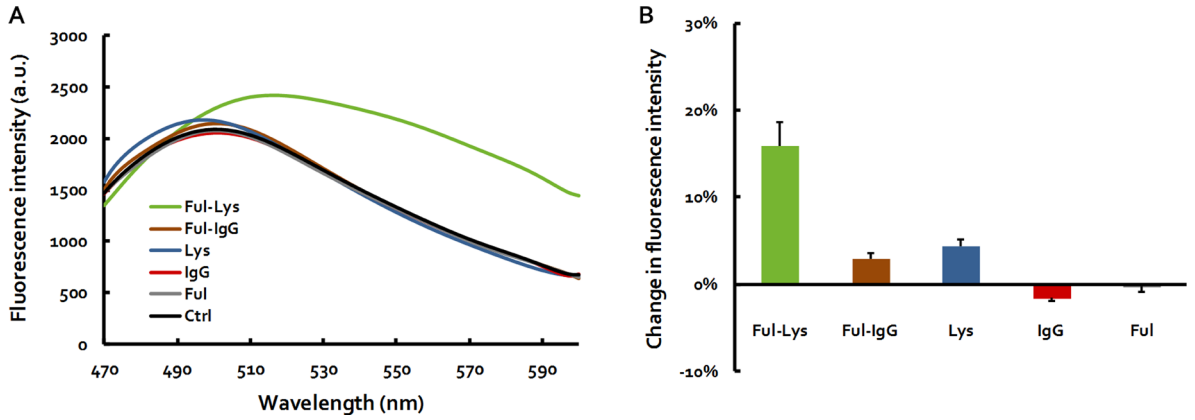

Figure 5. Thioflavin T assay on amyloid formation in proteins exposed to fullerol clusters. (A) Fluorescence emission spectra of IgG (0.1 mg/mL), lysozyme (0.01 mg/mL), and their mixture with fullerol clusters (0.03 mg/mL, corresponding to a NP:protein molar ratio of 50:1) after staining with a 50 μM Thioflavin T solution. Excitation wavelength: 440 nm. Control: Thioflavin T. (B) Changes in fluorescence intensity at peak wavelengths compared with the control.

that IgG and lysozyme are critical for host immunity, while the interactions of these proteins with cell surface receptors can exacerbate inflammation under certain circumstances.[26,31] Thus, a human acute monocytic leukemia cell line (THP-1), a commonly used model for mimicking the function and regulation of monocytes and macrophages and for immunocytochemical analysis, was selected to examine the immune responses of IgG and lysozyme upon their exposure to fullerol (Figure 6). Specifically, IgG, lysozyme, and fullerol controls at concentrations as high as 1 mg/mL induced a negligible immune response after incubating with THP-1 cells, as indicated by the cytokine TNF-α secretion level. However, the THP-1 cells displayed a completely different cytokine release after incubating with fullerol cluster−IgG and fullerol cluster−lysozyme. As indicated in the lower left panel in Figure 6, IgG did not elicit a notable effect on the THP-1 cells in the increased presence of fullerol clusters and similar amounts of inflammatory cytokines secretions were observed. This suggests that IgG did not undergo a significant conformational change upon fullerol binding, consistent with the DSF, CD, and Thioflavin T results. In contrast, increased fullerol concentrations promoted the interactions between lysozyme and the THP-1 cells to yield a progressively increased TNF-α secretion (Figure 6, low right panel). As evidenced in the literature, the aggregation of lysozyme can significantly alter their secondary structure to give rise to a high content of cross-β-sheets.[26] Such conformational change can be recognized by toll-like receptor (TLR)1/TLR2 heterodimer and activate the NF-κB pathways to trigger an elevated TNF-α secretion.[26] This result strongly agrees with our observations that fullerol induced significant changes in the secondary structure (CD) as well as amyloid fibrillation in lysozyme (DSF and Thioflavin T), which rendered an elevated immune response. It should be noted that the presence of cell culture medium, such as the case of this immunoassay, could impact the physicochemical properties as well as composition of nonspecific NP−protein complexes. However, as demonstrated in our recent proteomic studies with both carbon nanotubes and silver NPs in cell culture medium,[32,33] the complexity of such aspect is vast, while the controls of fullerol and proteins as well as the samples of fullerol:protein of various molar ratios in Figure 6 collectively pointed to the role of NP−protein binding as a plausible cause for the differential immune responses observed for IgG and lysozyme.

dx.doi.org/10.1021/jp506135m | J. Phys. Chem. C 2014, 118, 22069−22078

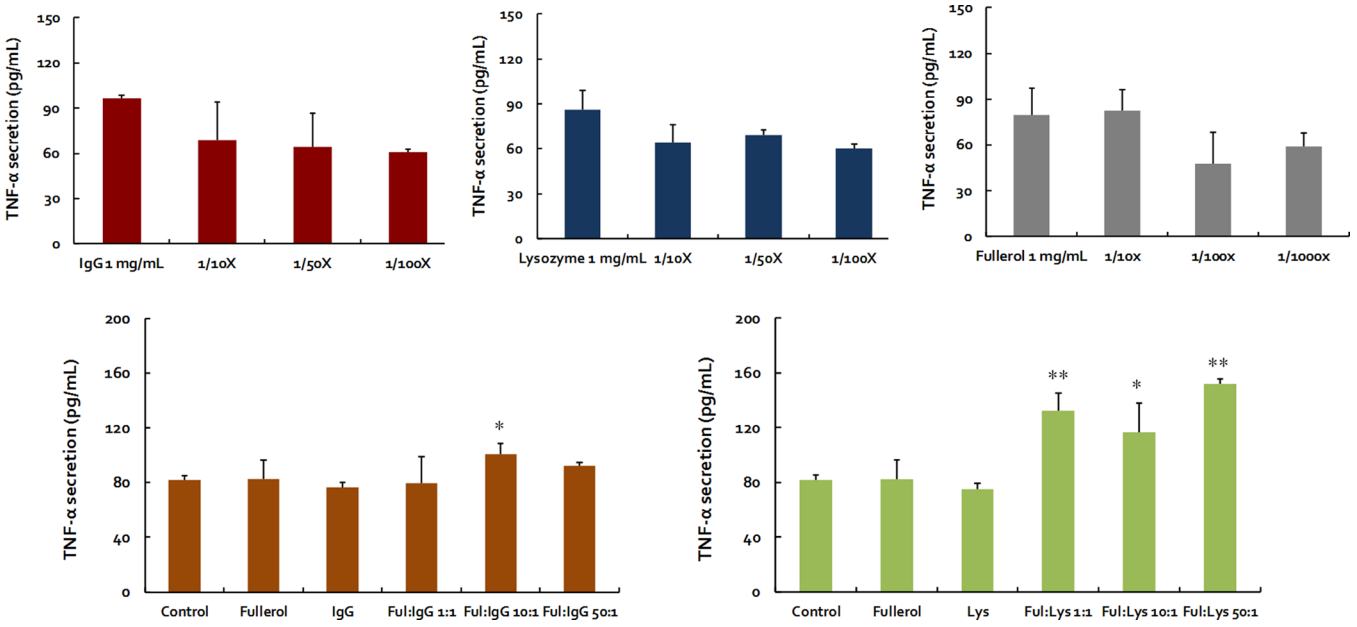

Figure 6. THP-1 cell immune responses to fullerol cluster−IgG and fullerol cluster−lysozyme. The top row shows TNF-α secretion in THP-1 cells in response to IgG (left), lysozyme (middle), and fullerol (right) stocks of 1 mg/mL and various dilutions (e.g., 1/10×: 10 times dilution of the stock), respectively. The bottom row shows TNF-α secretion in THP-1 cells in response to fullerol cluster−IgG (left) and fullerol cluster−lysozyme (right) of various molar ratios. Control: cytokine secretion in the absence of fullerol clusters and proteins. Fullerol: 100 mM (or 0.1 mg/mL). A NP:protein molar ratio of 50:1 corresponds to a fullerol concentration of 100 μM and a protein concentration of 2 μM (or 0.3 mg/mL for IgG and 0.03 mg/mL for lysozyme). Statistical analysis of experimental data with respect to the IgG and lysozyme controls: *: p value <0.05, **: p value <0.01 (Student t test).

CONCLUSIONS

We have shown using the methodologies of DSF, DLS, CD, Thioflavin T assay, docking simulations, and AlphaLISA immunoassays the contrasting effects of fullerol clusters on the stability of IgG and lysozyme. Our experiments suggest that NPs do not behave like ligands due to their duality, existing both as a particle and as a chemical. Such duality stems from the physicochemical properties of NPs, especially their limited solubility and finite size that are fundamentally different from a small organic ligand such as a drug or an endogenous biomolecule. While IgG and lysozyme possess comparable surface charge and amphiphilicity, IgG is tripodal in morphology and is comparable to fullerol clusters in size especially at elevated temperatures while lysozyme is globular and is significantly smaller. The disparities in protein size and morphology have been shown to involve two different biophysical mechanisms supported by the zeta potential measurement. The fullerol clusters interacted with the entirety of lysozyme to alter its prevailing α-helical content into a β-sheet dominant architecture through electrostatic forces and H-bonding, compromising the protein stability and function similarly to the phenomena of ubiquitin binding onto citrate-coated silver NPs.[23] The fullerol clusters stabilized IgG conforming to the general phenomenon of protein−ligand binding.[19] In this case, however, the fullerol clusters were likely situated at the IgG periphery (and vice versa) and stabilized the protein through hydrogen bonding and additional nonspecific forces that could be overcome by elevated temperatures. This latter scenario suggests a potential role reversal in certain NP−protein interactions to the rendition of a protein core and a NP corona, as noted in our discrete molecular dynamics simulations of the binding of ubiquitin and single fullerene derivatives.[34]

Our study has provided biophysical insights, some of which are consistent with the established paradigms of protein−ligand binding and NP−protein corona, and some of which are novel and surprising. One plausible conclusion from this study is that cell response to NPs is strongly influenced by changes in protein secondary structure. The manifold behaviors of NPs this current study has identified suggest that NPs could be used as enzyme inhibitors,[35−38] and as a novel nanomedicine for triggering tailored immune response and amyloid fibril formation. The effects of NPs may be further extended to inhibiting cancerous cell growth, adhesion, and division, since protein stability and flexibility are correlated[39] and both support the mechanics and assembly of cytoskeletal filaments by molecular machines. Methodologically, this study has demonstrated the potential of DSF as an effective, rapid, cost saving (i.e., small sample volumes of <20 μL), and high-throughput tool for examining the interfacial phenomena of NPs and biomolecular species whose implications extend to the fields of bioimaging, sensing, drug delivery, and safe nanotechnology.

EXPERIMENTAL AND COMPUTATIONAL METHODS

Sample Preparations. Polyhydroxyl fullerene $C_{60}(OH)_{20}$, or fullerol (MW 1060 Da), was purchased from BuckyUSA and was suspended in Milli-Q water to form a stock of 1 mg/mL (or ∼1 M). The fullerol suspension was bath-sonicated for 6 h (Unisonics Australia) and then filtered through a 0.2 μm membrane filter to remove large aggregates. Human IgG (MW ∼150 kDa) and hen-egg white lysozyme (MW 14 307 Da; isoelectric point 11.35) were purchased in lyophilized powder form from Sigma-Aldrich. The IgG was dissolved in 150 mM NaCl (pH 7.0) as recommended by the provider, while the lysozyme was directly dissolved in Milli-Q water (pH 7.4), both

dx.doi.org/10.1021/jp506135m | J. Phys. Chem. C 2014, 118, 22069−22078

to 1 mg/mL stock solutions, corresponding to 6.67 μM for IgG and 69.9 μM for lysozyme, respectively.

Hydrodynamic Size and Zeta Potential. The hydrodynamic diameters of the fullerol clusters, IgG, and lysozyme in water were determined by DLS (Zetasizer Nano S90, Malvern Instruments) at room temperature. The zeta potentials of the proteins, fullerol, and fullerol−proteins (1:1 weight ratio) in water were determined using the same device. To facilitate DSF data analysis a calibration curve of fullerol hydrodynamic size versus temperature was acquired using a DynaPro Plate Reader (Wyatt) (Supporting Information Figure S2).

DSF Assay. 96-well white PCR plates (Thermo Fisher AB0600/W) were used for the DSF measurements to determine the melting temperatures of IgG and lysozyme versus fullerol and NaCl of increasing concentrations. The volume of each sample well was fixed at 19.7 μL and, after 2 h of incubation, an additional 0.3 μL of a 10% (500×) of Sypro Orange was added to each well by an automated liquid dispenser (Phoenix, Art Robbins Instruments) to a total volume to 20 μL. For the salt dependence measurement a stock NaCl solution of 1 M was used to titrate into the final salt concentrations of 453 mM or less, for a fixed fullerol:protein molar ratio of 3:1. The samples were spun for 1 min at 1000 rpm (164 RCF, Centrifuge 5804) to ensure good mixing. The filled PCR plate was loaded into a Bio-Rad CFX96 optical reaction module attached to a C1000 thermal cycler, running the Bio-Rad CFX Manager 3.0 software on a Windows 7 computer. The thermal cycler was set to hold a temperature of 20 °C for 30 s before beginning a stepped heating cycle to 100 °C, of 0.5 °C every 5 s. At the end of each heating step, the optical reaction module collected data. Including data collection, the assay took approximately 45 min. The data was automatically processed at the end of each experiment using the CFX Manager software. Processed data was exported to Microsoft Excel. To ensure repeatability and statistics each sample condition was measured in triplicate. The interference from fullerol autofluorescence on the DSF measurements was negligible, as evidenced by the fullerol control (1 mg/mL) in Supporting Information Figure S4.

Docking Simulations. A molecular model of fullerene with 20 hydroxyl functional groups was constructed and energy minimized in preparation for the computational docking. X-ray crystal structures of hen egg white lysozyme (PDB ID: 4BAD) and human antibody IgG1 b12 (PDB ID: 1HZH) were prepared for docking with AutoDock Tools. Any ligands, heteroatoms, and crystallographic waters were removed from the protein structures prior to the docking. The search space for the docking on the protein structures was made sufficiently large to encompass the entire active site cavity for lysozyme and all the CDR loops of one of the Fab regions for IgG1. The exhaustiveness parameter was set at 200. The docking output from AutoDock Vina[40] was analyzed with AutoDock Tools and the ViewDock module of Chimera.[41]

Circular Dichroism Spectroscopy. To access the effects of fullerol cluster binding on the secondary structure of the proteins, spectra were recorded using a J-815 circular dichroism spectrometer (JASCO) for a quartz cuvette of 3 mm path length over a wavelength range of 195−300 nm at room temperature. Data were collected every 0.1 nm with a bandwidth of 1 nm at a scanning speed of 50 nm/min and averaged over three measurements. The protein samples were incubated with fullerol (0.03 mg/mL) for 2 h at room temperature before each measurement. The final spectra were baseline-corrected and the data were measured in mean residue ellipticity (θ) and converted to standard unit of deg·cm^2 dmol^{-1} using equation $[\theta] = (\theta \times M_0)/(10\,000 \times C_{soln} \times L)$, where M_0 denotes the mean residue molecular weight (114 g/mol), C_{soln} is the protein concentration (g/mL), and L is the path length through the buffer (cm).

Thioflavin T Assay. Protein samples (IgG of 0.1 mg/mL and lysozyme of 0.01 mg/mL) and their mixtures with fullerol clusters (0.03 mg/mL) were preincubated for 2 h before the addition of a 50 μM Thioflavin T solution (dissolved in 10 mM phosphate buffer, 150 mM NaCl, pH 7.0). A sample volume of 100 μL was added to each well in a 96-well white PCR plate. The samples were excited at 440 nm and their fluorescence spectra were recorded from 460 to 600 nm using a Systemmtic H1 plate reader (Bioteck) at a 2 nm scan step at room temperature. All the results were measured and averaged in triplicate.

Immunoassays. The immune responses of human THP-1 cells upon exposure to fullerol cluster−IgG and fullerol cluster−lysozyme were investigated by a homogeneous bead-based sandwich AlphaLISA immunoassay (PerkinElmer, Waltham, MA), which is based on photoinduced chemiluminescence between pairs of antibody-conjugated donor and acceptor beads (Scheme 1). The antibodies on donor and acceptor beads bind to different domains of the target analyte, forming a donor-analyte-acceptor sandwich structure to bring the donor and acceptor beads in close proximity (<200 nm). Upon excitation at 680 nm, singlet oxygens released from the donor beads diffuse and trigger a cascade of chemical events in the acceptor beads, resulting in a sharp chemiluminescence emission at 615 nm. Due to the diffusion length of the singlet oxygen, the emission signal is only generated when the analytes are captured by antibodies linked on both donor and acceptor beads.

In the experiment, cytokine TNF-α was selected as the target biomarker to evaluate the immune response of the THP-1 cells. Briefly, known concentrations of (0−5000 pg/mL) were spiked in RPMI medium and a TNF-α calibration curve was first obtained (Supporting Information Figure S6). Then, 8 μL of THP-1 cells with a total cell number of 20 000 in cell culture media were loaded into a 96 well plate. Two microliters of IgG−fullerol and lysozyme−fullerol solutions with different protein to NP molar ratios were injected into each well and incubated at 37 °C with 5% CO_2 for 4 h. Four microliters of a mixture of AlphaLISA acceptor beads (10 μg/mL) and biotinylated TNF-α antibody (10 nM) were added and incubated with the immune cells for 1 h, followed by addition of 6 μL of AlphaLISA streptavidin-coated donor beads (400 μg/mL). The 96-well plate was then incubated at 37 °C with 5% CO_2 for another 30 min. After that, the 96-well plate was placed on a customized inverted fluorescent microscope (Nikon Eclipse Ti−S, Nikon) for detection. A 500 mW 680 nm laser light (S-67-500C-100-H, Coherent, Clara, CA) was used to excite the AlphaLISA donor beads and the 615 nm emission signal was collected by an electron multiplying charge-coupled device (EMCCD) camera (Photometrics, Tucson, AZ) and analyzed by the NIS-Element BR analysis software.

■ ASSOCIATED CONTENT

Ⓢ Supporting Information

DSF melting curves, calibration of fullerol hydrodynamic size versus temperature and calibration of the AlphaLISA immuno-

assays. This material is available free of charge via the Internet at http://pubs.acs.org.

AUTHOR INFORMATION

Corresponding Authors

*E-mail: dave.winkler@csiro.au.
*E-mail: jason.kirby@csiro.au.
*E-mail: puchun.ke@csiro.au. Tel: 61-3-96627406.

Notes

The authors declare no competing financial interest.

ACKNOWLEDGMENTS

Ke acknowledges a DVS fellowship from the Office of Chief Executive at CSIRO. Kurabayashi acknowledges financial support from NSF Grant CBET 1263889. The authors thank the Australian Biotech Growth Partnership Theme for supporting the infrastructure needed to complete the experiments. The authors also thank Dr. Hong Yin for assistance with the zeta potential measurement and Dr. Janet Newman for comments on the manuscript. This research was sponsored by funding to the Nanosafety team at CSIRO.

REFERENCES

(1) Nel, A. E.; Madler, L.; Velegol, D.; Xia, T.; Hoek, E. M.; Somasundaran, P.; Klaessig, F.; Castranova, V.; Thompson, M. Understanding Biophysicochemical Interactions at the Nano-bio Interface. *Nat. Mater.* **2009**, *8*, 543−557.

(2) Maynard, A. D.; Aitken, R. J.; Butz, T.; Colvin, V.; Donaldson, K.; Oberdorster, G.; Philbert, M. A.; Ryan, J.; Seaton, A.; Stone, V.; et al. Safe Handling of Nanotechnology. *Nature* **2006**, *444*, 267−269.

(3) Ke, P. C.; Lamm, M. H. A Biophysical Perspective of Understanding Nanoparticles at Large. *Phys. Chem. Chem. Phys.* **2011**, *13*, 7273−7283.

(4) Lynch, I.; Dawson, K. A. Protein-Nanoparticle Interactions. *Nano Today* **2008**, *3*, 40−47.

(5) Vroman, L.; Adams, A. L.; Fischer, G. C.; Munoz, P. C. Interaction of High Molecular Weight Kininogen, Factor XII, and Fibrinogen in Plasma at Interfaces. *Blood* **1980**, *55*, 156−159.

(6) Cedervall, T.; Lynch, I.; Lindman, S.; Berggard, T.; Thulin, E.; Nilsson, H.; Dawson, K. A.; Linse, S. Understanding the Nanoparticle-Protein Corona Using Methods to Quantify Exchange Rates and Affinities of Proteins for Nanoparticles. *Proc. Natl. Acad. Sci. U.S.A.* **2007**, *104*, 2050−2055.

(7) Lundqvist, M.; Stigler, J.; Elia, G.; Lynch, I.; Cedervall, T.; Dawson, K. A. Nanoparticle Size and Surface Properties Determine the Protein Corona with Possible Implications for Biological Impacts. *Proc. Natl. Acad. Sci. U.S.A.* **2008**, *105*, 14265−14270.

(8) Hellstrand, E.; Lynch, I.; Andersson, A.; Drakenberg, T.; Dahlback, B.; Dawson, K. A.; Linse, S.; Cedervall, T. Complete High-Density Lipoproteins in Nanoparticle Corona. *FEBS J.* **2009**, *276*, 3372−3381.

(9) Salvati, A.; Pitek, A. S.; Monopoli, M. P.; Prapainop, K.; Bombelli, F. B.; Hristov, D. R.; Kelly, P. M.; Aberg, C.; Mahon, E.; Dawson, K. A. Transferrin-Functionalized Nanoparticles Lose Their Targeting Capabilities when a Biomolecule Corona Adsorbs on the Surface. *Nat. Nanotechnol.* **2013**, *8*, 137−143.

(10) Deng, Z. J.; Liang, M.; Monteiro, M.; Toth, I.; Minchin, R. F. Nanoparticle-Induced Unfolding of Fibrinogen Promotes Mac-1 Receptor Activation and Inflammation. *Nat. Nanotechnol.* **2011**, *6*, 39−44.

(11) Pantoliano, M. W.; Petrella, E. C.; Kwasnoski, J. D.; Lobanov, V. S.; Myslik, J.; Graf, E.; Carver, T.; Asel, E.; Springer, B. A.; Lane, P.; et al. High-Density Miniaturized Thermal Shift Assays as a General Strategy for Drug Discovery. *J. Biomol. Screen.* **2001**, *6*, 429−440.

(12) Niesen, F. H.; Berglund, h.; Vedadi, M. The Use of Differential Scanning Fluorimetry to Detect Ligand Interactions that Promote Protein Stability. *Nat. Protoc.* **2007**, *2*, 2212−2221.

(13) Seabrook, S. A.; Newman, J. High-Throughput Thermal Scanning for Protein Stability: Making a Good Technique More Robust. *ACS Comb. Sci.* **2013**, *15*, 387−392.

(14) Da Ros, T.; Prato, M. Medicinal Chemistry with Fullerenes and Fullerene Derivatives. *Chem. Commun.* **1999**, 663−669.

(15) Lin, C.-M. C60 Fullerene Derivatized Nanoparticles and Their Application to Therapeutics. *Recent Pat. Nanotechnol.* **2012**, *6*, 105−113.

(16) Ratnikova, T. A.; Govindan, P. N.; Salonen, E.; Ke, P. C. *In Vitro* Polymerization of Microtubules with a Fullerene Derivative. *ACS Nano* **2011**, *5*, 6306−6314.

(17) Brant, J. A.; Labille, J.; Robichaus, C. O.; Wiesner, M. Fullerol Cluster Formation in Aqueous Solutions: Implications for Environmental Release. *J. Colloid Interface Sci.* **2007**, *314*, 281−288.

(18) Kakinen, A.; Ding, F.; Chen, P.; Mortimer, M.; Kahru, A.; Ke, P. C. Interaction of Firefly Luciferase and Silver Nanoparticles and Its Impact on Enzyme Activity. *Nanotechnology* **2013**, *24*, 345101−1−9.

(19) Brandts, J. F.; Lin, L.-N. Study of Strong to Ultratight Protein Interactions Using Differential Scanning Calorimetry. *Biochemistry* **1990**, *29*, 6927−2940.

(20) Shrake, A.; Ross, P. D. Origins and Consequences of Ligand-Induced Multiphasic Thermal Protein Denaturation. *Biopolymers* **1992**, *32*, 925−940.

(21) Emsley, J. Very Strong Hydrogen Bonding. *Chem. Soc. Rev.* **1980**, *9*, 91−124.

(22) Maeda, Y.; Yamada, H.; Ueda, T.; Imoto, T. Effect of Additives on the Renaturation of Reduced Lysozyme in the Presence of 4 M Urea. *Protein Eng.* **1996**, *9*, 461−465.

(23) Ding, F.; Radic, S.; Chen, R.; Chen, P.; Geitner, N. K.; Brown, J. M.; Ke, P. C. Direct Observation of a Single Nanoparticle-Ubiquitin Corona Formation. *Nanoscale* **2013**, *5*, 9162−9169.

(24) Vertegel, A. A.; Siegel, R. W.; Dordick, J. S. Silica Nanoparticle Size Influences the Structure and Enzymatic Activity of Adsorbed Lysozyme. *Langmuir* **2004**, *20*, 6800−6807.

(25) Zhang, J. Protein-Protein Interactions in Salt Solutions, in *Protein-Protein Interactions − Computational and Experimental Tools*; Intech China: Shanghai, 2012; Chapter 18, pp 359−376.

(26) Gustot, A.; Raussens, V.; Dehousse, M.; Dumoulin, M.; Bryant, C. E.; Ruysschaert, J. M.; Lonez, C. Activation of Innate Immunity by Lysozyme Fibrils is Critically Dependent on Cross-β Sheet Structure. *Cell. Mol. Life Sci.* **2013**, *70*, 2999−3012.

(27) Ban, T.; Hamada, D.; Hasegawa, K.; Naiki, H.; Goto, Y. Direct Observation of Amyloid Fibril Growth Monitored by Thioflavin T Fluorescence. *J. Biol. Chem.* **2003**, *278*, 16462−16465.

(28) Ehrenberg, M. S.; Friedman, A. E.; Finkelstein, J. N.; Oberdorster, G.; McGrath, J. L. The Influence of Protein adsorption on Nanoparticle Association with Cultured Endothelial Cells. *Biomaterials* **2009**, *30*, 603−610.

(29) Shang, W.; Nuffer, J. H.; Dordick, J. S.; Siegel, R. W. Unfolding of Ribonuclease A on Silica Nanoparticle Surfaces. *Nano Lett.* **2007**, *7*, 1991−1995.

(30) Lynch, I.; Salvati, A.; Dawson, K. A. Protein−Nanoparticle Interactions: What Does the Cell See? *Nat. Nanotechnol.* **2009**, *4*, 546−547.

(31) Fernández-Calotti, P. X.; Salamone, G.; Gamberale, R.; Trevani, A.; Vermeulen, M.; Geffner, J.; Giordano, M. Downregulation of Mac-1 Expression in Monocytes by Surface-Bound IgG. *Scand. J. Immunol.* **2003**, *57*, 35−44.

(32) Shannahan, J. H.; Brown, J. M.; Chen, R.; Ke, P. C.; Lai, X.; Mitra, S.; Witzmann, F. A. Comparison of Nanotube-Protein Corona Composition in Cell Culture Media. *Small* **2013**, *9*, 2171−2181.

(33) Shannahan, J. H.; Lai, X.; Ke, P. C.; Podila, R.; Brown, J. M.; Witzmann, F. A. Silver Nanoparticle Protein Corona Composition in Cell Culture Media. *PLoS One* **2013**, *8*, e74001−1−10.

(34) Radic, S.; Govindan, P. N.; Chen, R.; Salonen, E.; Brown, J. M.; Ke, P. C.; Ding, F. The Effect of Fullerenol Surface Chemistry on

Nanoparticle Binding-Induced Protein Misfolding. *Nanoscale* **2014**, *6*, 8340−8349.
(35) Tzoupis, H.; Leonis, G.; Durdagi, S.; Mouchlis, V.; Mavromoustakos, T.; Papadopoulos, M. G. Binding of Novel Fullerene Inhibitors to HIV-1 Protease: Insight Through Molecular Dynamics and Molecular Mechanics Poisson−Boltzmann Surface Area Calculations. *J. Comput.-Aided Mol. Des.* **2011**, *25*, 959−976.
(36) Friedman, S. H.; DeCamp, D. L.; Sijbesma, R. P.; Srdanov, G.; Wudl, F.; Kenyon, G. L. Inhibition of the HIV-1 Protease by Fullerene Derivatives: Model Building Studies and Experimental Verification. *J. Am. Chem. Soc.* **1993**, *115*, 6506−6509.
(37) Govindan, P. N.; Monticelli, L.; Salonen, E. Mechanism of *Taq* DNA Polymerase Inhibition by Fullerene Derivatives: Insight from Computer Simulations. *J. Phys. Chem. B* **2012**, *116*, 10676−10683.
(38) Winkler, D. A.; Burden, F. R.; Yan, B.; Weissleder, R.; Tassa, C.; Shaw, S.; Epa, V. C. Modeling and Predicting the Biological Effects of Nanomaterials. *SAR QSAR Environ. Res.* **2014**, *25*, 161−172.
(39) Celej, M. S.; Montich, G. G.; Fidelio, G. D. Protein Stability Induced by Ligand Binding Correlates with Changes in Protein Flexibility. *Protein Sci.* **2003**, *12*, 1496−1506.
(40) Trott, O.; Olson, A. J. AutoDock Vina: Improving the Speed and Accuracy of Docking with a New Scoring Function, Efficient Optimization, and Multithreading. *J. Comput. Chem.* **2010**, *31*, 455−461.
(41) Pettersen, E. F.; Goddard, T. D.; Huang, C. C.; Couch, G. S.; Greenblatt, D. M.; Meng, E. C.; Ferrin, T. E. UCSF Chimera–A Visualization System for Exploratory Research and Analysis. *J. Comput. Chem.* **2004**, *25*, 1605−1612.